BIOCHEMISTRY
including biophysical chemistry & molecular biology

Article

pubs.acs.org/biochemistry

Ligand Access to the Active Site in *Thermus thermophilus* ba_3 and Bovine Heart aa_3 Cytochrome Oxidases

William McDonald,[†] Chie Funatogawa,[†] Yang Li,[‡] Istvan Szundi,[†] Ying Chen,[‡] James A. Fee,[‡] C. David Stout,[‡] and Ólöf Einarsdóttir*[,†]

[†]Department of Chemistry and Biochemistry, University of California, Santa Cruz, California 95064, United States

[‡]Department of Molecular Biology, The Scripps Institute, MB-8, 10550 North Torrey Pines Road, La Jolla, California 92037, United States

Supporting Information

ABSTRACT: Knowledge of the structure and dynamics of the ligand channel(s) in heme-copper oxidases is critical for understanding how the protein environment modulates the functions of these enzymes. Using photolabile NO and O_2 carriers, we recently found that NO and O_2 binding in *Thermus thermophilus* (*Tt*) ba_3 is ∼10 times faster than in the bovine enzyme, indicating that inherent structural differences affect ligand access in these enzymes. Using X-ray crystallography, time-resolved optical absorption measurements, and theoretical calculations, we investigated ligand access in wild-type *Tt* ba_3 and the mutants, Y133W, T231F, and Y133W/T231F, in which tyrosine and threonine in the O_2 channel of *Tt* ba_3 are replaced by the corresponding bulkier tryptophan and phenylalanine, respectively, present in the aa_3 enzymes. NO binding in Y133W and Y133W/T231F was found to be 5 times slower than in wild-type ba_3 and the T231F mutant. The results show that the *Tt* ba_3 Y133W mutation and the bovine W126 residue physically impede NO access to the binuclear center. In the bovine enzyme, there is a hydrophobic "way station", which may further slow ligand access to the active site. Classical simulations of diffusion of Xe to the active sites in ba_3 and bovine aa_3 show conformational freedom of the bovine F238 and the F231 side chain of the *Tt* ba_3 Y133W/T231F mutant, with both residues rotating out of the ligand channel, resulting in no effect on ligand access in either enzyme.

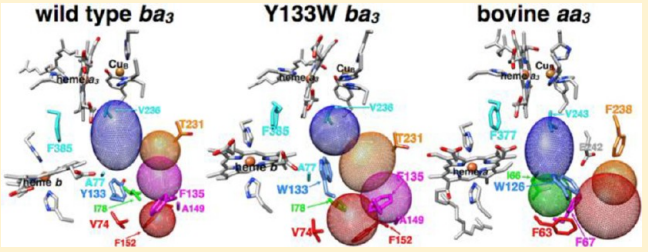

During the evolution of metalloenzymes and their catalytic activity, the protein environment was likely to have been modified in such a way that it effectively tuned ligand pathways and metal-based prosthetic group(s) for optimal function under different conditions. The heme-copper oxidases play a key role in energy production of aerobic organisms,[1−3] and their structural and functional similarities and differences make them an ideal system for exploring the effect of the protein environment on enzymatic function. The heme-copper oxidases have been classified into three subfamilies, A, B, and C, based on their phylogenetic and structural analysis.[4,5] The A-family bacterial *Rhodobacter sphaeroides* (*Rs*) and *Paracoccus denitrificans* (*Pd*) aa_3 oxidases are highly homologous in sequence to their mitochondrial counterpart,[5] while other heme-copper oxidases, including the B-family *Thermus thermophilus* (*Tt*) ba_3[6] and the C-family cbb_3 oxidases,[7] are phylogenetically more distant, with a low degree of sequence homology to the aa_3 oxidases.[5] Phylogenetic analysis has shown that the A-family is the most ancient, with both the B- and C-families evolving later.[8]

The heme-copper oxidases catalyze the reduction of O_2 to water, which is coupled to the generation of a transmembrane electrochemical proton gradient required for ATP synthesis.[1−3] Previous heme-copper oxidase research focused on the mechanisms of electron and proton transfer,[1−3] but less emphasis has been placed on the pathway(s) through which O_2 and other small ligands, such as NO and CO, move to the binuclear active site. A primary question concerns the structural and dynamic differences responsible for the adaptation of the heme-copper oxidases to different functional environments. For example, the Gram-negative bacterium *T. thermophilus* grows optimally at 70 °C[9] and is found under microaerobic conditions, such as those existing at high temperatures, at oxic−anoxic interfaces, or in hypersaline microbial mats.[8] The *Tt* HB8 strain has adapted to these environments as a facultative anaerobe[10] and has been shown to express two types of oxidases depending on the oxygen tension.[10,11] The B-type ba_3 oxidase has a higher oxygen affinity and is typically expressed under microaerobic conditions (∼10 μM), while the lower-oxygen affinity A-type caa_3 oxidase is expressed at higher oxygen concentrations.[12−14]

On the basis of their crystal structures, putative O_2 channels have been suggested for the bovine heart aa_3 enzyme,[15] *Rs* aa_3,[16] *Pd* aa_3,[17] *Tt* ba_3,[6] *Escherichia coli* (*E. coli*) bo_3,[18] and

Received: October 4, 2012
Revised: December 21, 2012
Published: January 2, 2013

Pseudomonas stutzeri cbb_3.[7] Mutagenesis and biochemical experiments with *Rs* aa_3, *Pd* aa_3, and *E. coli* bo_3 suggest that these channels may indeed serve as paths for diffusion of ligands into the binuclear site.[19,20] The residues and helices lining the channels demonstrate significant sequence and structural similarity among the different heme-copper oxidases.[5] However, the global structure of the catalytic subunit shows structural variations that may be related to different physiological and biochemical roles. A recent crystallographic study of the binding of xenon (Xe) to *Tt* ba_3 identified a "Y-shaped" hydrophobic channel, 18−20 Å in length, leading from the protein exterior of subunit I to the binuclear center; the channel is defined by five major and two minor discrete Xe atom binding sites (Xe1−Xe7).[21,22] Moreover, there is a narrowing caused by conserved tryptophan and phenylalanine residues in the ligand channel of the bovine, *Rs*, and *Pd* aa_3 oxidases,[16,20,23] while smaller residues, tyrosine (Y133) and threonine (T231) occupy these sites in *Tt* ba_3[6,21] (Figure 1).

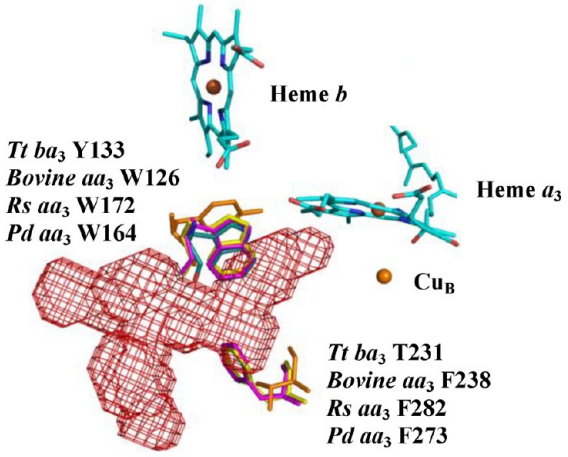

Figure 1. Superimposition of the constriction residues, tryptophan and phenylalanine, of bovine aa_3 (cyan sticks), *Rs* aa_3 (yellow sticks), and *Pd* aa_3 (magenta sticks) onto the corresponding residues, Y133 and T231, respectively, of wild-type cytochrome ba_3 oxidase (orange sticks). The red mesh represents the oxygen channel. The volumes were calculated with VOIDOO.[21]

Considering the different functional environments of *Tt* ba_3 and the bovine heart cytochrome oxidase, one might expect not only structural but also kinetic differences between the two enzymes. At low oxygen concentrations (<5−10 μM), the rate of O_2 binding would be rate-limiting for O_2 reduction, assuming the bimolecular rate constant of 1×10^8 M^{-1} s^{-1} reported for the aa_3 enzymes. Although O_2 diffusion may be more efficient at higher temperatures because of increased protein dynamics, it may not be able to compensate for this rate-limited O_2 binding. Using photolabile O_2 and NO carriers in conjunction with time-resolved optical absorption (TROA) spectroscopy, we recently demonstrated that the binding of O_2 and NO in *Tt* ba_3 (1×10^9 M^{-1} s^{-1}) is 10-fold faster than in the bovine enzyme (1×10^8 M^{-1} s^{-1}).[24,25] These results suggest inherent differences between ligand access in the two enzymes, possibly related to the constriction point that is present in the aa_3 oxidases but absent in *Tt* ba_3. Hence, the more open O_2 channel in *Tt* ba_3 may reflect evolutionary adaptation in *Tt* ba_3 to increase the rate of diffusion of O_2 to the binuclear center, allowing the enzyme to maintain physiologically relevant reaction rates at low or microaerobic O_2 concentrations.

In this study, we used time-resolved optical absorption spectroscopy to investigate NO binding in *Tt* ba_3 single mutants Y133W and T231F and double mutant Y133W/T231F, in which the conserved tryptophan and phenylalanine residues in the ligand channel of the bovine, *Rs*, and *Pd* aa_3 enzymes are inserted into *Tt* ba_3. The results, together with the crystal structures of wild-type and mutant *Tt* ba_3 and classical simulations of diffusion of Xe into the active site of bovine aa_3 and *Tt* ba_3, provide strong support for the tryptophan (W126) constriction point residue and a hydrophobic pocket in the ligand channel of the bovine enzyme impeding access of NO to the active site in this enzyme but not in *Tt* ba_3.

MATERIALS AND METHODS

Protein Expression, Purification, and Crystallization. Recombinant wild-type and mutant (Y133W, Y133F, T231F, and Y133W/T231F) cytochrome ba_3 oxidase genes were expressed in *Tt* HB8 and the enzymes purified as previously described.[26] The proteins were concentrated to 20 mg/mL in 20 mM Tris buffer (pH 7.6) containing 0.05% *n*-dodecyl β-D-maltoside and stored at 4 °C.

Steady-State Activity Measurements. The steady-state activity of the *Tt* ba_3 mutants was measured using an oxygen electrode.[26] Purified *Tt* cytochrome c_{552} in 10 mM Tris buffer (pH 7.6) was first added to the reaction chamber to generate a flat baseline. This was followed by addition of 6 μL of 1.2 M ascorbate to obtain a background slope reading. After ∼1 min, 5 μL of the ba_3 sample (1 mg/mL) was added and the slope recorded until all the O_2 in the chamber had been consumed. The slope of the background was subtracted from the slope obtained during O_2 consumption; the resulting slope was used to calculate the steady-state activity.

Crystallization. The protein samples were spun at 15000*g* for 15 min prior to starting the crystallization trials. After centrifugation, the protein was mixed with monoolein (Sigma) in a 2:3 (v/v) ratio and homogenized with a syringe mixer.[27,28] Crystallization trials were performed in a 24-well hanging drop plate using 200 nL of protein-laden LCP (lipidic cubic phase) overlaid with 3 μL of reservoir solution.[29] The crystallization plates were stored at 20 °C. Crystals were obtained after incubation for several days in 50 mM sodium cacodylate buffer (pH 6.5) containing 1.6 M NaCl, and 40−42% poly(ethylene glycol) 400. Crystals were harvested and immediately flash-frozen in liquid nitrogen.

X-ray Data Collection and Structure Determination. Crystallographic data were collected at the Stanford Synchrotron Radiation Lightsource. Data sets were integrated, scaled, and merged using iMosflm.[30] The wild-type *Tt* ba_3 structure [Protein Data Bank (PDB) entry 3S8F] was used as the model for molecular replacement with Phaser.[31] The resulting models were adjusted manually in Coot and refined with Refmac5.[32] Crystallographic statistics for the refined structures of the Y133W and Y133W/T231F mutants are listed in Table S1 of the Supporting Information. Y133W and Y133W/T231F were deposited as PDB entries 4EV3 and 4ESL, respectively. The structure of the Y133F mutant was also determined at 2.80 Å resolution (PDB entry 4F05).

Time-Resolved Optical Absorption Measurements. The time-resolved optical absorption measurements were carried out using a CCD detector in combination with a photolabile NO carrier as previously described.[24] The data were subjected to singular value decomposition (SVD) and global exponential fitting, which provided the spectral changes (*b*-

dx.doi.org/10.1021/bi301358a | *Biochemistry* 2013, 52, 640−652

spectra) and the apparent lifetimes.[33−36] The intermediate spectra were extracted on the basis of a proposed mechanism and compared to model spectra of the proposed intermediates.

Classical Molecular Dynamics Simulations of Diffusion of Xe to the Binuclear Active Site in *Tt* ba_3 and Bovine aa_3. Classical molecular dynamics simulations of diffusion of Xe through subunit I of wild-type *Tt* ba_3, the Y133W and Y133W/T231F ba_3 mutants, and bovine aa_3 were performed using the following protocol. Initial coordinates for the bovine enzyme were taken from the 1.90 Å resolution reduced enzyme crystal structure (PDB entry 2EIJ),[37] and those for *Tt* ba_3 were obtained from the 2.30 Å resolution oxidized enzyme crystal structure (PDB entry 1XME);[38] no significant side chain movements or backbone displacements are observed upon comparison of ba_3 crystal structures in different redox states.[39] The initial conformations of the Y133W tryptophan and T231F phenylalanine side chains were obtained from the crystal structure published in this work after root-mean-square deviation (rmsd) fitting of the mutants to the simulated structure of an equilibrated wild-type model. The enzyme models contain subunit I from each structure, which includes the low-spin heme *a*/*b* (bovine/*Tt* ba_3, respectively), high-spin heme a_3, and Cu_B. The bovine enzyme includes a Mg^{2+} ion. All lysine and arginine residues were positively charged, and all histidine residues were neutral. Aspartate residues and heme propionates were negatively charged, and except for the bovine Glu242, glutamate residues were negatively charged. The proteins were inserted into a lipid bilayer consisting of two leaflets of 64 dimyristoylphosphatidylcholine lipid molecules (DMPC) each and then capped with TIP3P water molecules. The bovine enzyme model was then made neutral by the addition of seven Na^+ ions, while wild-type *Tt* ba_3, Y133W, and Y133W/T231F models were neutralized with five Cl^- ions. The final wild-type ba_3, Y133W and Y133W/T231F ba_3 mutant, and bovine aa_3 simulations included 42457, 42460, 42466, and 35817 atoms, respectively.

The first three production simulations, 1 ns in duration, were started from the equilibrated system by placing a Xe atom in the Xe1, Xe2, and Xe5 binding sites of *Tt* ba_3 subunit I identified in ref 21. Subsequent simulations were continuations of these first three. Equivalent Xe binding sites were identified in the bovine enzyme by structure alignment with wild-type *Tt* ba_3 using the MatchMaker function in UCSF Chimera.[40] Cavities were determined by binning all trajectories according to the average distance from Xe to Cu_B (see Table S2 of the Supporting Information). Within each bin, the maximal and minimal distances from Xe to Cu_B and from Xe to two additional residues were calculated (W128 and F67 for bovine, Y133 and I78 for wild-type ba_3, and W133 and I78 for the Y133W mutant). The ranges of distances were then adjusted to remove double counting of time points while maximizing the time during which Xe was in a respective cavity. Additional details regarding the simulation protocol and system preparation and equilibration can be found in the Supporting Information.

RESULTS

Structures and Steady-State Activities of the O_2 Channel Mutants. The O_2 diffusion channel in wild-type *Tt* ba_3, as defined by the crystallographic occupancy of Xe atoms,[21] is shown in Figure 1 in relation to Y133 and T231. These residues are superimposed on the corresponding tryptophan and phenylalanine residues, respectively, in bovine aa_3 (cyan), *Rs* aa_3 (yellow), and *Pd* aa_3 (magenta). In Figure 2, Y133 and T231 of wild-type *Tt* ba_3 are superimposed on W133 and F231

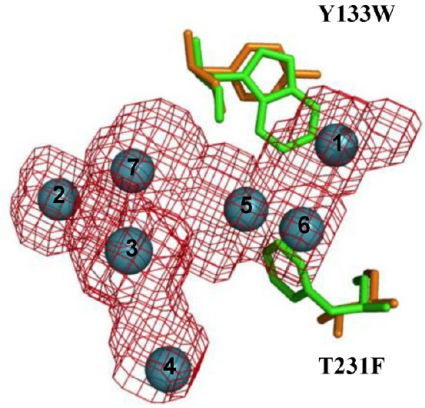

Figure 2. Comparison of wild-type ba_3 and the Y133W/T231F mutant showing constriction of the O_2 diffusion channel. The red mesh represents the computed oxygen channel as in Figure 1. Blue spheres represent seven gas binding sites observed in Xe-pressurized *Tt* ba_3 crystals.[21] Orange sticks represent residues Y133 and T231 of wild-type *Tt* ba_3 and green sticks residues W133 and F231 of the Y133W/T231F double mutant.

in the structure of the Y133W/T231F double mutant, showing how each of the larger side chains intrudes into the channel and the binding sites of three Xe atoms (see also Figure S1 of the Supporting Information). Overall, the structures of wild-type ba_3 and the Y133W and Y133W/T231F mutants are very similar (rmsd of subunit I Cα atoms of 0.18−0.25 Å). The principal difference at residue 133 is a change of the χ_2 torsion angle by ∼30° such that the tryptophan side chain rotates away from a propionate of heme a_3, normally engaged in a hydrogen bond with Y133, and in so doing provides a hydrogen bond from the indole to the propionate. Consequently, the tryptophan extends into the channel while maintaining a key interaction with heme a_3. It also displaces the H_2O molecule present in the native structure that is bridged to the active site via another bound H_2O. The tryptophan side chain positions in the structures of the single and double mutants are virtually identical. The shortest atom−atom distances between W133 and Cu_B are 8.44 and 8.43 Å for the single and double mutant, respectively.

The principal difference at residue 231 due to substitution of phenylalanine for threonine is a 0.67 Å displacement of Cβ. A hydrogen bond from T231 to the amide of L200 in an adjacent α-helix is lost while the phenylalanine side chain gains hydrophobic contacts with W193, L200, and I235 at the interface of helices V and VI. Furthermore, the replacement of threonine with phenylalanine in the double mutant results in a shortest atom−atom distance between W133 and F231 of 5.1 Å, compared to the distance of 7.3 Å between W133 and T231.

The steady-state activities of Y133W, T231F, and Y133W/T231F were found to be 57, 82, and 70%, respectively, of that of recombinant wild-type ba_3. While the rate of O_2 binding is unlikely to limit the steady-state kinetics under the room-temperature experimental conditions, this may not be the case at the low O_2 concentrations under which the enzyme is expressed.

Binding of NO to Reduced Wild-Type ba_3 and Its Constriction Mutants. The reaction of NO with fully reduced recombinant wild-type *Tt* ba_3 and the Y133W, T231F, and

Y133W/T231F ba_3 mutants (hereafter termed the constriction mutants) was investigated in the absence of CO using a photolabile NO carrier.[24] Recent studies in our laboratory have shown that NO binds to wild-type *Tt* ba_3 with the same rate as O_2, suggesting that the two ligands follow the same ligand path and that NO serves as a good mimic for O_2 binding but without the complexities of the subsequent microsecond time scale redox reactions.[24] Using the NO photolabile carrier also circumvents the low NO quantum yield in NO flash-photolysis studies, the rate limitation of conventional NO stopped-flow methods, and, importantly, the recently reported interference from the photodissociated CO when using the CO flow-flash method.[24,25] Figure 3 (A–C) shows the time-resolved

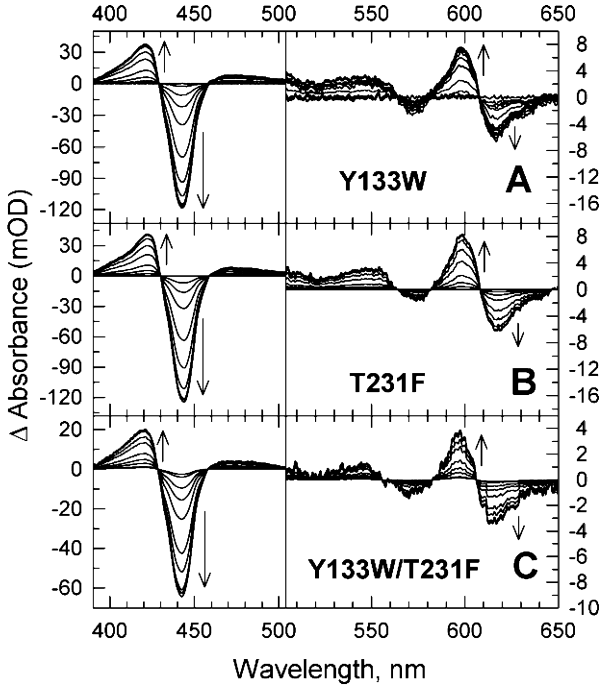

Figure 3. Time-resolved optical absorption difference spectra recorded during the reaction of photoproduced NO with the reduced *Tt* ba_3 mutants: Y133W (A), T231F (B), and Y133W/T231F (C). The experiments were conducted with 2 mM ascorbic acid and 1 μM phenazine methosulfate (PMS). The absorbance difference spectra are those obtained following subtraction of the spectral contribution of the photolabile NO complex, determined in a separate experiment. The spectra were recorded at logarithmically spaced delay times between 1 μs and 5 ms (A), 200 ns and 200 μs (B), and 1 μs and 1 ms (C). The effective enzyme concentrations were 2.5 μM (A), 2.8 μM (B), and 1.4 μM (C). The NO concentrations were 85 μM (A), 120 μM (B), and 110 μM (C).

difference spectra recorded during the reaction of the photoproduced NO with the reduced *Tt* ba_3 mutants, Y133W (panel A), T231F (panel B), and Y133W/T231F (panel C). The absorbance difference spectra are those obtained following subtraction of the spectral contribution of the photolabile NO complex, determined in a separate experiment.

Figure 4 shows the NO binding kinetics at 444 nm, the absorbance maximum of the reduced heme a_3, for recombinant wild-type ba_3 (■), Y133W (○), T231F (□), Y133W/T231F (●), and bovine aa_3 (▲); the absorption has been normalized to 1. The data are from the multiwavelength data presented above and are plotted on a logarithmic time scale. Clearly, mutating Y133 in ba_3 to the corresponding tryptophan

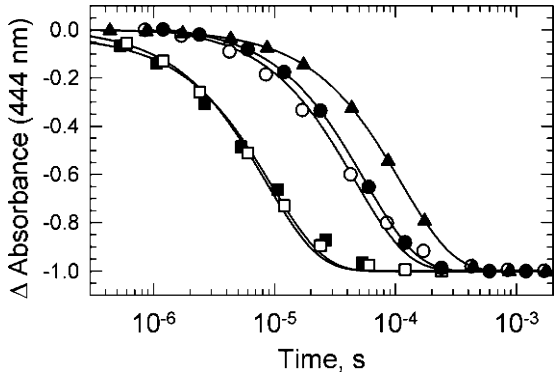

Figure 4. NO binding kinetics at 444 nm for wild-type *Tt* ba_3 (■), T231F (□), Y133W (○), Y133W/T231F (●), and bovine aa_3 (▲). The traces are plotted on a logarithmic time scale, with the maximal absorbance difference values normalized to 1. The experimental time dependence has been converted to correspond to the same NO concentration for each sample (100 μM). The solid lines represent the calculated traces obtained on the basis of global exponential fits.

constriction residue in the aa_3 oxidases (W126 in the bovine enzyme) significantly reduces the rate of NO binding, although not to the level observed in the bovine enzyme; however, this is not the case for the T231F mutation, an issue addressed in more detail below. The solid lines represent the calculated traces obtained on the basis of global exponential fits discussed below.

SVD-based global exponential fitting of the time-resolved absorption spectra recorded during the reaction of NO with the Y133W, Y133W/T231F, and T231F *Tt* ba_3 mutants revealed apparent lifetimes of 54 μs (85 μM NO), 46 μs (110 μM NO), and 7.1 μs (120 μM NO), respectively. These lifetimes represent binding of NO to the reduced heme a_3, an assignment based on the spectral changes, and show a linear dependence on NO concentration. The lifetimes correspond to second-order rate constants of 2.2×10^8, 2.0×10^8, and $\sim 1 \times 10^9$ M^{-1} s^{-1} for the Y133W, Y133W/T231F, and T231F *Tt* ba_3 mutants, respectively. The second-order rate constant for binding of NO to recombinant wild-type ba_3 was found to be $\sim 1 \times 10^9$ M^{-1} s^{-1}, which is equal to our previously reported second-order rate constant for the nonrecombinant wild-type enzyme.[24] In contrast, the analogous rate for the bovine enzyme is $\sim 1 \times 10^8$ M^{-1} s^{-1}.[24,41] Thus, the rate of NO binding in the Y133W and Y133W/T231F mutants is approximately ~5 times slower than that observed for wild-type *Tt* ba_3, while it is unaffected by the T231F mutation.

Classical Simulations of Diffusion of Xe to the Active Site in *Tt* ba_3 and Bovine aa_3. To explore ligand access to the binuclear site in *Tt* ba_3 and bovine aa_3, we performed multiple 1 ns classical molecular dynamics simulations of a xenon (Xe) atom diffusing through subunit I of the enzymes immersed in a dimyristoylphosphatidylcholine (DMPC) bilayer and capped with TIP3P water molecules (see Materials and Methods and Supporting Information for details). The Xe atom was chosen to be consistent with the crystallographic experiments of refs 21 and 22 and because it is nonpolar and its van der Waals radius is similar to that of O_2; however, Xe can be described entirely by a nonbonded potential in the classical simulations. The interface of subunits I and III of the bovine enzyme has recently been suggested to provide an entry point for dioxygen.[42] While subunit III (and subunit II) is absent from the simulations, this does not alter the global

dx.doi.org/10.1021/bi301358a | *Biochemistry* 2013, 52, 640–652

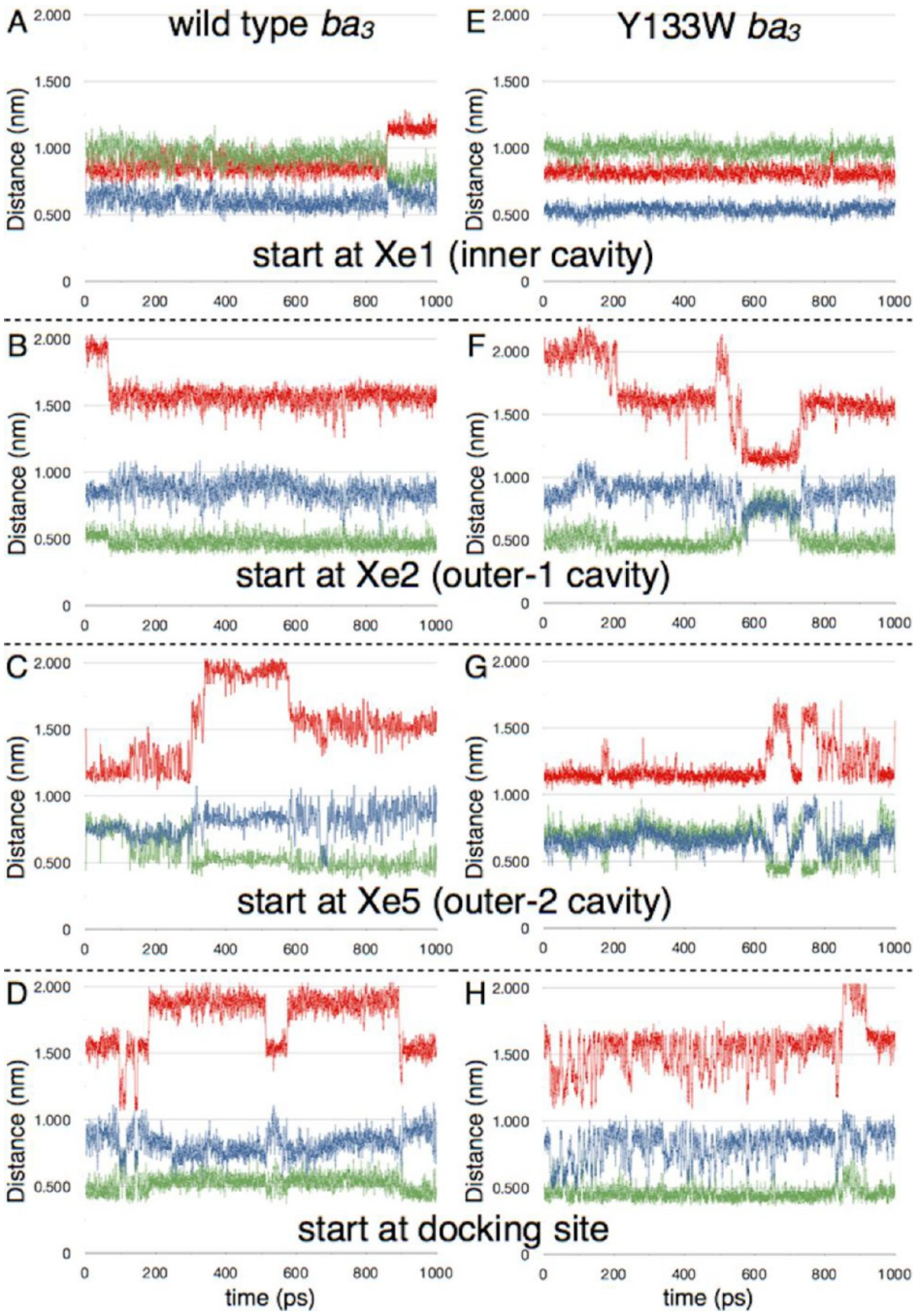

Figure 5. Representative time series of the Xe−Cu_B distance (red), the Xe−Y133 distance (blue), and the Xe−I78 distance (green) for wild-type ba_3 (A−D) and the Y133W mutant (E−H). The Xe atom was initially placed at (A and E) the Xe1 site in the inner cavity, (B and F) the Xe2 site in the outer1 cavity, (C and G) the Xe5 site in the outer2 cavity, and (D and H) the docking site.

structure of subunit I as evidenced by root-mean-square fluctuations (rmsf) in simulated Cα positions of 2.64 ± 0.08 Å relative to the crystal structure. Consequently, the absence of subunits II and III is not expected to alter the size or location of cavities within the catalytic subunit.

Diffusion of Xe through the Channel in Wild-Type *Tt* ba_3 and the Y133W and Y133W/T231F Mutants. Xe diffusion within the ligand channel of wild-type *Tt* ba_3 and its Y133W and Y133W/T231F mutants was monitored using the following three distances: (1) the distance from Xe to Cu_B, (2) the distance from Xe to Y(W)133, and (3) the distance from Xe to I78. The time series for the Xe−Cu_B (red trace), Xe−Y(W)133 (blue trace), and Xe−I78 (green trace) distances for four representative trajectories each for wild-type *Tt* ba_3 (panels A−D) and the Y133W mutant (panels E−H) are presented in Figure 5. The time series of the three distances for both the wild-type enzyme and the mutants suggest that the ligand channel may be divided into four regions, presented graphically in panels A and B of Figure 6 for the wild-type enzyme and panels C and D of Figure 6 for the Y133W mutant; panels A and C and panels B and D represent a view from the P-side of the membrane and from within the membrane, respectively. These regions include an inner cavity (blue spheres and ellipsoids), two outer cavities, hereafter termed outer1 (red

dx.doi.org/10.1021/bi301358a | *Biochemistry* 2013, 52, 640−652

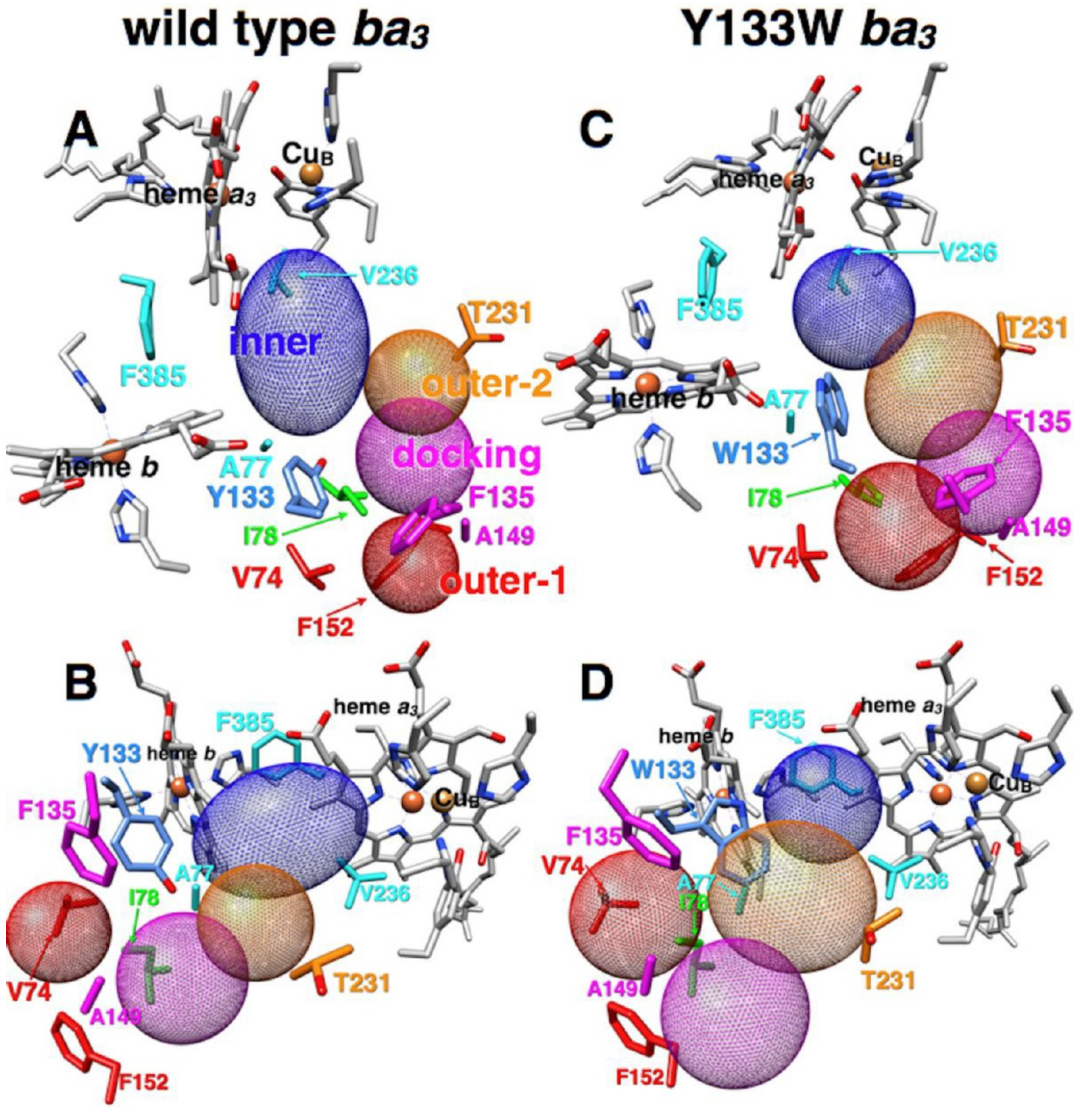

Figure 6. Four regions of the wild-type *Tt* ba_3 (A and B) and Y133W (C and D) ligand channel: inner cavity (blue spheres and ellipsoids), the outer1 cavity (red spheres), and the outer2 cavity (orange spheres). The magenta spheres represent the docking site between the outer1 and outer2 cavities as viewed from (A and C) the P-side of the membrane and (B and D) within the membrane. Y(W)133 is colored blue, and I78 is colored green.

spheres) and outer2 (orange spheres), and a docking site (magenta spheres) between the outer1 and outer2 cavities; comparative studies of the bovine enzyme will be discussed separately below. The distances defining these cavities are listed in Tables S2A and S2B of the Supporting Information for wild-type ba_3 and the Y133W mutant, respectively. As is clear from Figure 6, the Y133W mutation does alter the ligand channel in significant ways to be discussed in detail below.

The Y133W mutation has little effect on the dimensions and position of the outer1 cavity (Figure 6, red spheres), and this is confirmed by the simulations (see Table S2 of the Supporting Information). However, the increased steric bulk of the tryptophan compared to the native tyrosine decreases the volume of the inner cavity (blue spheres) as reflected by a comparison of the distances in Table S2A and S2B of the Supporting Information. Furthermore, in the Y133W mutant, the inner cavity moves "up" in the protein, i.e., closer to the P-side of the membrane, compared to its position in the wild-type enzyme. While the inner cavity in the Y133W mutant is still bounded by F385 on helix IX as in wild-type ba_3, a Xe atom does not approach A77 as in the wild-type enzyme. Rather, it stops within van der Waals contact of W133 (the site of the point mutation) and stays somewhat "above" V236, closer to W229 on helix VI. The outer2 cavity (Figure 6, orange spheres) in the Y133W mutant is elongated and increased in volume compared to that of the wild-type enzyme (compare Table S2A to Table S2B of the Supporting Information), and while still bounded by T231, the outer2 cavity stretches from W133 to F135 in the mutant. The volume of the docking site between the outer1 and outer2 cavities is decreased, and the docking site is pushed "lower" (i.e., closer to the N-side of the membrane) in the Y133W mutant than in the native enzyme (Figure 6, magenta spheres).

The occupation times of the inner, outer1, and outer2 regions and the docking site in wild-type ba_3 and the Y133W mutant, expressed as a percentage of simulation time, are listed in Tables 1 and 2, respectively. For the trajectories in which the Xe was placed in the outer2 cavity, the occupation time of the inner cavity in the mutant simulations (Table 2) is half of that of the wild-type enzyme (Table 1), while the level of retention

dx.doi.org/10.1021/bi301358a | *Biochemistry* 2013, 52, 640−652

Table 1. Times of Occupation (% simulation time) of the Four Regions of the Wild-Type ba_3 Ligand Channel

		time of occupation[a] (%)			
no. of simulations	initial Xe placement	inner cavity	outer1	docking site	outer2
4	inner cavity	95 (7)	0	0	5 (7)
4	outer1	0	71 (44)	29 (44)	0
5	docking site	0	34 (35)	62 (32)	4 (6)
6	outer2	11 (28)	21 (39)	14 (18)	54 (39)

[a]Values in parentheses are standard deviations.

Table 2. Times of Occupation (% simulation time) of the Four Regions of the Y133W ba_3 Ligand Channel

		time of occupation[a] (%)			
no. of simulations	initial Xe placement	inner cavity	outer1	docking site	outer2
4	inner cavity	77 (46)	0	1 (2)	22 (45)
5	outer1	0	46 (20)	49 (19)	5 (6)
4	docking site	0	26 (31)	48 (41)	25 (50)
5	outer2	5 (11)	0	8 (11)	87 (12)

[a]Values in parentheses are standard deviations.

in the outer2 cavity increases from 54 to 87% in the presence of W133. These results suggest that the movement of the Xe atom between the inner and outer2 cavities is more restricted in the Y133W mutant. The same behavior is observed in simulations of the Y133W/T231F mutant (not shown).

Diffusion of Xe through the Ligand Channel in the Bovine aa_3 Enzyme. While the Y133W mutation in *Tt* ba_3 slows the rate of NO binding 5-fold, it alone is not solely responsible for the observed 10-fold difference in ligand binding between wild-type *Tt* ba_3 and the bovine enzyme. To explore this issue further, we conducted comparative simulations of diffusion of a Xe atom to the active site in the bovine enzyme. The diffusion of Xe within the internal cavity of the bovine enzyme was followed using the three distances, analogous to that of the ba_3 enzyme: (1) the distance from Xe to Cu_B, (2) the distance from Xe to W126 (one of the two constriction residues), and (3) the distance from Xe to F67 [the bottom residue of the hydrophobic pocket identified in our simulations (see below)]. The bovine W126 and F67 residues correspond to wild-type *Tt* ba_3 Y133 and I78 residues, respectively. The time evolutions of the Xe−Cu_B (red trace), Xe−W126 (blue trace), and Xe−F67 (green trace) distances for four representative trajectories of the bovine enzyme are presented in Figure 7A−D. From the time series of these three distances, we suggest that the ligand channel may be divided into four regions, presented graphically in panels E and F of Figure 7, an inner cavity (blue ellipsoids), an outer1 cavity (red spheres), an outer2 cavity (orange spheres), and a hydrophobic pocket (green spheres) that separates the inner cavity from the outer1 cavity.

The time of occupation of each region, expressed as a percentage of the simulation time, is presented in Table 3. A Xe atom placed in the hydrophobic pocket tends to remain there (~76% of the time). Similarly, a Xe atom placed in the outer2 cavity remains in the outer2 cavity (88% of the time). Furthermore, the standard deviations in retention times for the simulations in which the Xe was initially placed in the hydrophobic pocket and outer2 cavity are small [14 and 12%, respectively (Table 3)], reflecting a consistent level of high occupancy across the simulations. These observations, combined with the narrow range of distances sampled by Xe, suggest that the hydrophobic pocket and, secondarily, the outer2 cavity are well-defined "docking" sites in the ligand channel of the bovine enzyme.

The ~15 Å Xe−Cu_B distance of the last 900 and 400 ps of the wild-type ba_3 trajectories in panels B and C of Figure 5, respectively, and the initial Xe placement in Figure 5D within the docking site are similar to the Xe−Cu_B distances to the hydrophobic pocket of the bovine enzyme (Figure 7D, red trajectory). However, the bovine hydrophobic pocket is in van der Waals contact with W126 and above F67, in contrast to the docking site of the ba_3 simulations, which is in contact with I78 and somewhat lower in the cavity than Y133 (compare Figures 6 and 7). Furthermore, the volume swept out by the Xe in the docking site of the wild-type ba_3 enzyme is larger than the volume sampled by Xe in the hydrophobic pocket of the bovine enzyme (Table S3 of the Supporting Information). Moreover, the standard deviation in the occupation time of the wild-type ba_3 docking site is large [32% (see Table 1)] compared to the standard deviation in the occupation time of the bovine hydrophobic pocket [14% (Table 3)], suggesting that the ba_3 docking site is less stable than the hydrophobic pocket of the bovine enzyme. It should be noted that for simulations in which the Xe was placed in the outer2 cavity, the occupation times of the ba_3 Y133W mutant (Table 2) are similar to those of the bovine enzyme (Table 3), suggesting that the Y133W mutation and the native bovine W126 restrict passage of the ligand between the inner and outer2 cavities. The volume of the inner cavity in the Y133W mutant is also decreased relative to that in the wild-type enzyme and is closer to that of the bovine enzyme (Table S3 of the Supporting Information). Furthermore, while the ligand channel is passive and the Xe simulations are dynamic with all the restraints removed (see Materials and Methods), both the crystal structures and the simulations show that ligand access in the Y133W and Y133W/T231F mutants and the bovine enzyme is impeded because the tryptophan residue extends into the middle of the cavity; we suggest that the presence of a hydrophobic pocket in the bovine enzyme further reduces the rate of ligand binding in this enzyme.

DISCUSSION

Effect of the Y133W Mutation on Ligand Access in *Tt* ba_3. Our recent time-resolved optical absorption studies show ~10 times faster rates of O_2 and NO binding in wild-type *Tt* ba_3 than in the bovine enzyme,[24,25] a result attributed to the narrower ligand channel in the bovine enzyme compared to that in *Tt* ba_3. The shortest distance across the O_2/NO channel in the crystal structures of the bovine enzyme, *Rs* aa_3, and *Pd* aa_3 is that between the tryptophan (W126) and phenylalanine (F238) residues, 4.6 Å (PDB entries 2EIJ,[37] 3FYE,[43] and 3HB3,[44] respectively), while in wild-type ba_3, the shortest distance (atom−atom) between the corresponding but less bulky Y133 and T231 residues is 10.4 Å (PDB entry 3S8F). Neither Y133 nor T231 extends into the ligand channel cavity in wild-type ba_3 based on its crystal structure, and in the molecular dynamics Xe simulations, the side chains of Y133 and T231 have approximately the same orientations as in the crystal structure (side chain fluctuations of ~1 Å). In the bovine enzyme, the corresponding tryptophan (W126) and phenylalanine (F238) both extend into the ligand channel (Figure 1), suggesting that the slower ligand access in this enzyme arises

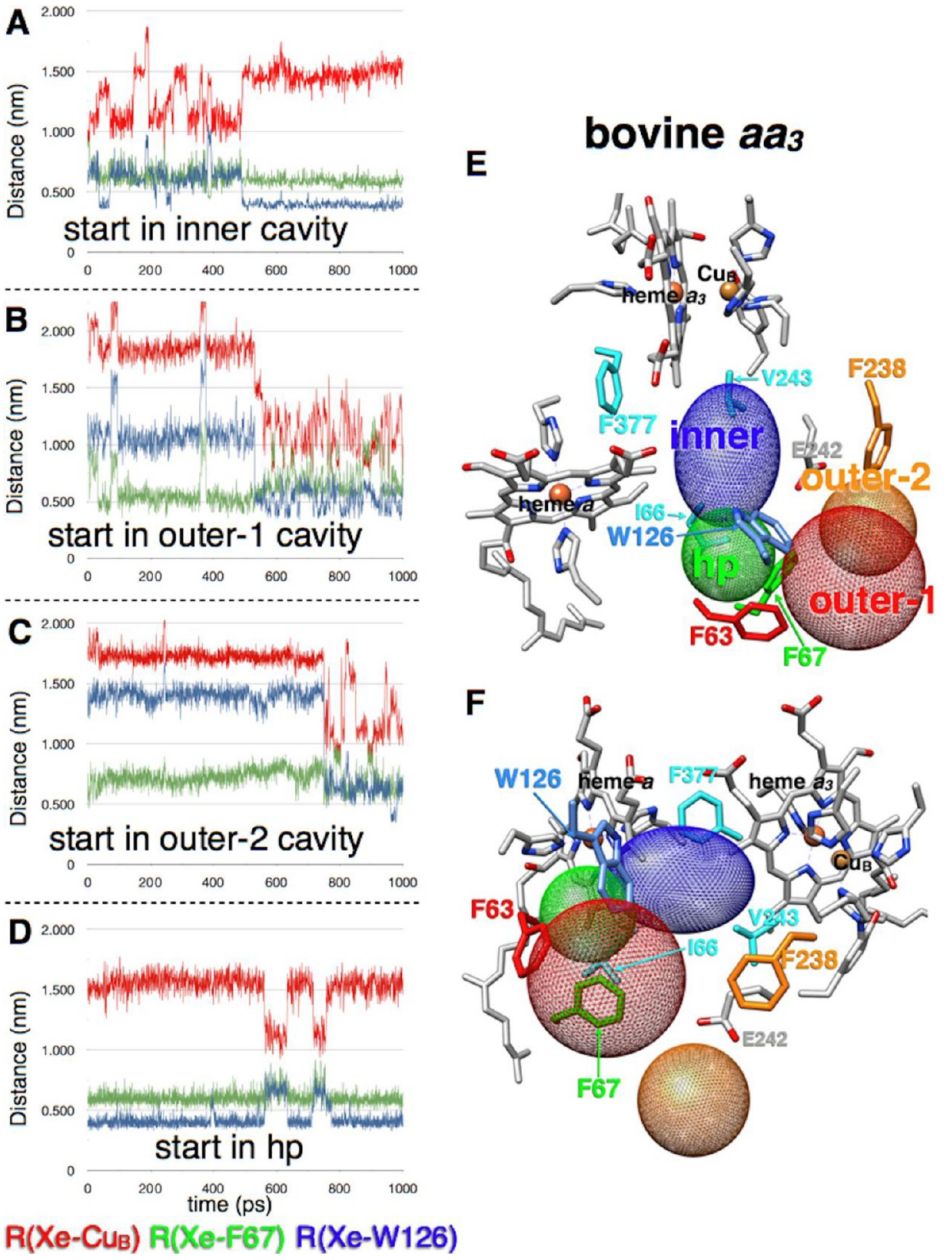

Figure 7. (A–D) Representative time series of the Xe–Cu_B distance (red), the Xe–W126 distance (blue), and Xe–F67 distance (green) for the bovine enzyme. The Xe atom was initially placed (A) in the inner cavity, (B) in the outer1 cavity, (C) in the outer2 cavity, and (D) in the hydrophobic pocket (hp). (E and F) Four regions of the bovine ligand channel: the inner cavity (blue ellipsoids), the hydrophobic pocket (hp) (green spheres), the outer1 cavity (red spheres), and the outer2 cavity (orange spheres) as viewed from (E) the P-side of the membrane and (F) within the membrane. W126 is colored blue, and F67 is colored green.

Table 3. Times of Occupation (% simulation time) of the Four Regions of the Bovine aa_3 Ligand Channel

		time of occupation[a] (%)			
no. of simulations	initial Xe placement	inner cavity	pocket	outer1	outer2
7	inner cavity	55 (21)	34 (20)	9 (12)	0
4	pocket	19 (15)	76 (14)	0	0
5	outer1[b]	7 (16)	2 (4)	33 (39)	2 (1)
6	outer2	2 (6)	1 (2)	6 (9)	88 (12)

[a]Values in parentheses are standard deviations. [b]The data in this row do not sum to 100% because in two of five simulations the Xe atom escapes from the cavity interior into the lipids and is not within the ligand channel of the protein.

from the constriction point present in the oxygen channel of the aa_3 oxidases but absent in *Tt* ba_3.

The time-resolved optical absorption results reported in this study demonstrate that mutating Y133 of *Tt* ba_3 to the corresponding tryptophan constriction residue present in the ligand channel of the aa_3 oxidases significantly (5 times) slows access of NO to the active site in the mutant and, by inference, in the aa_3 enzymes. This is consistent with the crystal structure of the *Tt* ba_3 Y133W mutant, which shows that replacing Y133 of ba_3 with the corresponding tryptophan residue physically constricts the ligand channel (Figure 2). The molecular dynamics simulation of diffusion of Xe into the active site in the Y133W mutant shows that the tryptophan residue maintains the same orientation during the simulation as in

dx.doi.org/10.1021/bi301358a | *Biochemistry* 2013, 52, 640–652

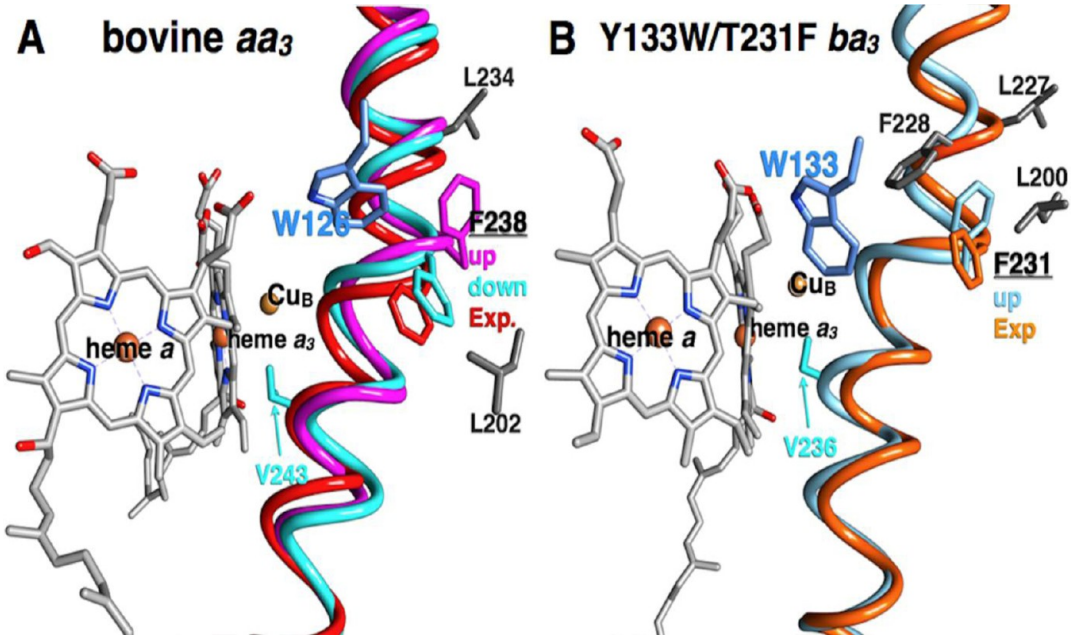

Figure 8. Comparison of the conformations of the bovine aa_3 F238 and *Tt* ba_3 F231 side chains observed in the crystal structures (exp) to those in the molecular dynamics simulations. (A) The bovine crystal structure is colored red. (B) The Y133W/T231F mutant crystal structure is colored orange.

the crystal structure, with small side chain fluctuations of 0.8−1.1 Å. Y133 in wild-type ba_3, W133 in the Y133W mutant, and W126 in the bovine enzyme are all oriented to maintain the H-bond to the propionate. In our simulations, the H-bond is more transient in the Y133W mutant; i.e., the time-averaged H-bond distance is longer than that in the wild-type enzyme, and the W133 residue is twice as likely to be separated by distances outside the H-bonding range compared to Y133. While the differences are small, they do demonstrate the transient and dynamic nature of the hydrogen bonding observed in crystal structures at 100 K. As discussed below, the Y133W mutation alters the ligand channel compared to the wild-type enzyme by decreasing the volume of some cavities while increasing the volume of others.

Role of the F231 Side Chain Dynamics in Ligand Access in the Y133W/T231F Mutant. In contrast to the Y133W mutant, the mutation of T231 of *Tt* ba_3 to the corresponding phenylalanine "constriction" residue present in the bovine enzyme had no effect on the rate of binding of NO to heme a_3. However, the crystal structure of the Y133W/T231F mutant shows that F231 partially blocks the ligand channel (Figure 2). This suggests that the dynamics of residue 231 must play an important role in ligand access to the active site in the T231F mutant. This proposal is supported by our molecular dynamics simulations of the Y133W/T231F mutant (see below). Furthermore, the *b* factors for the wild-type T231 side chain are smaller than the average *b* factor for the respective protein, while the *b* factors for the F231 side chain are larger than the average *b* factor for the double mutant. This suggests increased positional variability in the phenylalanine side chain of the Y133W/T231F mutant; this is also true for the T231F single mutant.

During the simulation of wild-type ba_3, the T231 residue is positioned near the bottom edge of the outer2 cavity (Figure 6A,B). The rmsfs in atomic positions for the T231 side chain are small, ranging from 0.7 to 1.1 Å, with the largest motions belonging to CH_3 rotation. This indicates that T231 is rigid, in accordance with a hydrogen bond between the side chain and the amide of L200, and does not extend into the cavity. However, this is not the case for F231 in the respective mutants. In the simulation of the Y133W/T231F mutant, the F231 residue changes its conformation from that in the crystal structure, with the side chain rotating up (pointing toward the P-side of the membrane) with a χ_1 torsion angle of −70° (this torsion angle is 11.3° in the crystal structure presented here) (Figure 8, right panel). As a result of this repacking, F231 no longer extends into the cavity but strengthens the contacts with L200 and F228 on helices V and VI, respectively. These hydrophobic contacts may compensate for the loss of the T231−L200 hydrogen bond and explain the limited range of conformers of F231. In none of the simulations does the Xe atom interact with F231. Rotations of aromatic side chains have been observed in molecular dynamics simulations. For example, rapid equilibration of aromatic side chains is observed in the "relaxed-complex" method for ligand docking simulations.[45] Furthermore, the E92Q/N155H and G140S/Q148H HIV-I integrase double mutants significantly alter the distribution of the conformations of H67,[46] a residue that is crucial to virulence.[47]

Dynamics of the F238 Constriction Residue in the Bovine Enzyme. In the bovine crystal structure, F238 extends into the ligand channel (Figure 1). During the molecular dynamics simulation of the bovine enzyme, the F238 constriction point residue lies higher in the ligand channel, i.e., closer to the P-side of the membrane, in relation to the outer2 cavity (Figure 7E and F) while T231 of ba_3 is located at the lower edge of the ba_3 outer cavity (Figure 6A). In the bovine enzyme, the F238 side chain adopts two conformations with χ_1 torsion angles of 55 ± 9° [down, (Figure 8A, colored cyan)] and −70 ± 8° [up (Figure 8A, colored magenta)], with occupation times of 63 and 37%, respectively; this angle is 27° in the published bovine crystal structure.[37] The conformer with the higher occupation time (55°) is that pictured in Figure 7 (E and F). The rotation of the F238 side chain down (i.e., toward

the N-side of the membrane) relative to the crystal structure places the F238 side chain between helices V and VI, in contact with L202. The alternative conformation rotates the F238 side chain up (i.e., toward the P-side of the membrane) relative to the crystal structure, in contact with L234 (Figure 8A); F231 in the Y133W/T231F ba_3 mutant adopts a conformation analogous to the up conformation of the bovine enzyme (Figure 8B). In neither conformation does bovine F238 interact with the Xe atom, which suggests that this residue does not interact with a diatomic ligand. Hence, the simulations show conformational freedom of phenylalanine at this position in the O_2 channel in both bovine aa_3 and *Tt* ba_3, which is not observed in the crystal structures.

Molecular Simulations of Xe Diffusion versus Xe Sites in the Crystal Structure of *Tt* ba_3. In recent freeze-trap, kinetic crystallography experiments with Xe-laden *Tt* ba_3 crystals, the migration of Xe from the internal channel was modeled by following the Xe crystallographic occupancy of five major crystallographic Xe binding sites (Xe1−Xe5).[22] While the volumes swept out by a Xe atom in our simulations are larger than the crystallographic binding sites and encompass more than one site (see Table S3 of the Supporting Information for the volumes of the cavities), in general, the locations of the principal sites in the crystal structures and simulations are in accord, with the Xe1, Xe2, and Xe5 binding sites being within the inner cavity, outer1 cavity, and outer2 cavity, respectively. The position of the Xe4 site overlaps our docking site, but the Xe4 and Xe3 sites lie closer to the N- and P-sides of the membrane, respectively, and are closer to the protein exterior than our docking site.

Hydrophobic Sink in the Bovine Enzyme. In agreement with previous simulations, we find that the internal ligand channel of the bovine oxidase is divided into several cavities.[23] As observed by Hofacker and Schulten,[23] the region near H151 on helix IV (our outer2 cavity) provides access to the inner cavity and an escape from the protein interior (Figure 7C, first 200 ps). We also find that in the bovine enzyme, a ligand is able to exit−and presumably enter−the protein through the outer1 cavity (Table 3). This is in agreement with the results of Xe-pressurized *Rs* aa_3 crystallographic studies suggesting that two cavities, the first near L157, I104, A153, and L105 (S116, F63, L112, and V64 in bovine numbering, respectively) and connecting to our outer1 cavity between helices II and III and the second near W172, F108, L246, and I250 (W126, F67, L202, and I206 in bovine numbering, respectively), in rough correspondence to our outer1 cavity, provide possible oxygen channels.[16] Significantly, on the basis of our classical simulations, we have identified a "sink" in the bovine enzyme that traps a Xe atom in a hydrophobic pocket between the inner and outer cavities at Cu_B distances of ∼15 Å. We propose that this trapping of the ligand, together with the constriction created by W126, gives rise to the 10-fold decrease in the rate of ligand binding in the bovine enzyme compared to that in *Tt* ba_3.

This previously unobserved hydrophobic pocket consists of residues F63, I66, F67, and W126 (Figure 7A,B). It should be noted that these residues define the edges of the volume that the Xe explores. The corresponding residues in *Tt* ba_3 are V74, A77, I78, and Y133, respectively, obtained by comparing the published crystal structure to that of the bovine enzyme (Table S2 of the Supporting Information). Bovine F63 and I66 are replaced by the much smaller V74 and A77, respectively, in ba_3. In *Tt* ba_3, the smaller V74 and A77 side chains (and G73) create a larger cavity, but it is occupied by a structural water molecule that is hydrogen bonded to two main chain atoms and a heme *b* propionate; presumably, this more polar environment excludes Xe.

Docking Sites in *Tt* ba_3 and Its Mutants. In contrast to the bovine enzyme, the *Tt* ba_3 enzyme does not seem to contain a hydrophobic pocket. Rather, we identify a well-defined docking site between the outer1 and outer2 cavities in ba_3 (Figure 6, magenta spheres). In ba_3, the top and bottom residues of the bovine enzyme hydrophobic pocket, W126 and F67, respectively, are reduced in steric bulk to Y133 and I78, respectively, and the ligand is free to diffuse within the inner cavity and into the binuclear center. According to the classical simulations, the Xe atom moves from the outer1 cavity in *Tt* ba_3 to the relatively stable docking site between the outer1 and outer2 cavities. From this site, the ligand in the wild-type enzyme has straight unhindered access to the binuclear center and can move fairly easily between the docking site and the outer1 and outer2 cavities, and the inner cavity as reflected by the large standard deviations in occupation times (Table 1) and the many passes Xe makes between the docking site and the other cavities.

As discussed above, our simulations indicate a relatively stable docking site in *Tt* ba_3 at the intersection of the outer1 and outer2 cavities (Figure 6, magenta spheres). The classical simulations of Varotsis and co-workers identified a docking site in the inner cavity of *Tt* ba_3, close to the ring propionate of heme a_3.[48] This site corresponds to the initial placement of Xe at the Xe1 site in the inner cavity (Figures 2 and 5A). As the ligand stays in this site for 900 ps before moving to the outer2 cavity, we cannot eliminate this site as a docking site. However, the inner cavity identified in our simulations encompasses twice the volume (100 $Å^3$) of the docking site at the intersection of the outer1 and outer2 cavities (49 $Å^3$) (see Tables S2A and S3 of the Supporting Information), as reflected by the larger range of distances sampled by the Xe atom in the inner cavity (Table S2A of the Supporting Information). However, the two results are not necessarily inconsistent as the simulations of Varotsis and co-workers[48] are 1 order of magnitude shorter than those represented here, which would preclude the observation of the ligand escaping from the inner cavity to the outer2 cavity or the nearby docking site.

As with wild-type ba_3, the Y133W mutant does not seem to contain a hydrophobic pocket with the same relative position within the ligand channel as in the bovine enzyme (compare Figures 6C,D and 7E,F). This highlights the importance of bovine F67 in defining this structural motif. However, the Y133W mutation significantly alters the ligand channel relative to the wild-type enzyme, decreasing the volume of the inner cavity from 100 to 48 $Å^3$ and increasing the volume of the outer2 cavity from 24 to 80 $Å^3$ (see Table S3 of the Supporting Information). Furthermore, the increased occupation time and decreased standard deviation in the occupation time of the outer2 cavity in all the Y133W ba_3 simulations (Table 2) compared to those of the wild type (Table 1), suggest that the outer2 cavity is a more stable docking site in the mutant.

Our simulations suggest that a ligand entering the protein interior via the outer1 cavity of the Y133W mutant moves with high probability into the docking site located between the outer1 and outer2 cavities (Figure 6C,D). From this site, a ligand is equally likely to move forward into the outer2 cavity or backward to the outer1 cavity (Table 2). However, the outer2 cavity presents a stable docking site to the nonpolar Xe, and

presumably O_2, and once a ligand occupies this site, the ligand is less likely to move to the inner cavity of the mutant compared to that of the wild-type enzyme. This reduced probability seems to result from the interaction of the Xe atom with W133 and F135, located in an extended loop above the ligand channel, and W229, a residue that π-stacks to H282, a ligand to Cu_B, providing a structural basis for the reduced ligand binding rate in the Y133W ba_3 enzyme compared to that in the wild-type enzyme (Figure 6).

CONCLUSIONS

Several conclusions can be drawn from our studies. First, our results demonstrate that mutation of the Y133 residue in the ligand channel of *Tt* ba_3 to the bulkier tryptophan residue present in the bovine enzyme impedes access of Xe to the active site in the Y133W and Y133W/T231F mutants. It can be inferred that the tryptophan constriction residue in the bovine enzyme at least partially controls the accessibility of the ligand to the active site in the bovine aa_3 oxidase. Second, the molecular dynamics simulations show that the F231 side chain, which in the Y133W/T231F crystal structure extends into the ligand channel, rotates out of the ligand channel, resulting in no effect on the rate of NO binding in the T231F mutant. This reflects the importance of protein dynamics in controlling access of the ligand to the active site. Third, the molecular dynamics simulations of diffusion of Xe into the active site in wild-type *Tt* ba_3, the Y133W and Y133W/T231F ba_3 mutants, and the bovine enzyme show that protein cavities or "docking sites" appear to be important in controlling the accessibility of the ligand to the active site. In particular, we have identified a hydrophobic pocket in the bovine enzyme that is absent in the thermophilic enzyme. We propose that this hydrophobic sink in the bovine enzyme traps the ligand, further decreasing the rate of ligand binding. Moreover, the top and bottom residues of the hydrophobic pocket of the bovine enzyme, W126 and F67, respectively, are conserved in *Rs* aa_3, *Pd* aa_3, and *E. coli* bo_3, suggesting these residues may define similar ligand cavities in these enzymes. In contrast, ba_3 does not contain a hydrophobic pocket. Consequently, the inner cavity is effectively larger than that in the bovine enzyme, which is characterized by distances to Cu_B of 5−10 Å; in the *Tt* ba_3 Y133W mutant, the volume of the inner cavity is decreased and is closer to that of the bovine enzyme. The absence of the constriction point and hydrophobic pocket in wild-type *Tt* ba_3 allows the ligand to diffuse freely into the binuclear center in this enzyme and provides a structural and dynamic basis for the differences in ligand binding between the aa_3 oxidases and cytochrome ba_3 from *T. thermophilus*. These differences likely reflect evolutionary adaptation of the *Tt* ba_3 to microaerobic conditions.

ASSOCIATED CONTENT

Supporting Information

Additional details regarding the simulation protocol and system preparation and equilibration for the classical molecular dynamic simulation, *Tt* ba_3 Y133W/T231F mutant in the context of the overall structure of the enzyme (Figure S1), a summary of data collection parameters and refinement statistics for the Y133W and Y133W/T231F mutants (Table S1), distances defining the regions of the ligand channels in wild-type *Tt* ba_3, Y133W *Tt* ba_3, and bovine aa_3 (Table S2), volumes of the cavities in the ligand channels of wild-type *Tt* ba_3, Y133W *Tt* ba_3, and bovine aa_3 (Table S3). This material is available free of charge via the Internet at http://pubs.acs.org.

Accession Codes

Y133F, Y133W, and Y133W/T231F deposited as PDB entries 4GP4, 4GP5, and 4GP8, respectively.

AUTHOR INFORMATION

Corresponding Author

*E-mail: olof@ucsc.edu. Fax: (831) 459-2935. Phone: (831) 459-3155.

Author Contributions

W.M., C.F., and Y.L. contributed equally to this work.

Funding

This work is supported by National Institutes of Health Grant GM53788 (ARRA supplement) and National Science Foundation Grant CHE-1158548 to Ó.E., and National Institutes of Health Grant GM035342 to J.A.F.

Notes

The authors declare no competing financial interest.

ACKNOWLEDGMENTS

Portions of this research were conducted at the Stanford Synchrotron Radiation Lightsource (SSRL), a Directorate of SLAC National Accelerator Laboratory and an Office of Science User Facility operated for the U.S. Department of Energy Office of Science by Stanford University. The SSRL Structural Molecular Biology Program is supported by the U.S. Department of Energy Office of Biological and Environmental Research and by the National Institutes of Health, National Institute of General Medical Sciences (including Grant P41GM103393), and the National Center for Research Resources (Grant P41RR001209).

ABBREVIATIONS

SVD, singular-value decomposition; *b* spectrum, spectral changes associated with an apparent rate (lifetime); *Tt* ba_3, *T. thermophilus* ba_3 cytochrome oxidase; *Rs*, *R. sphaeroides*; *Pd*, *P. denitrificans*.

REFERENCES

(1) Brzezinski, P., and Larsson, G. (2003) Redox-driven proton pumping by heme-copper oxidases. *Biochim. Biophys. Acta 1605*, 1−13.

(2) Ferguson-Miller, S., and Babcock, G. T. (1996) Heme/copper terminal oxidases. *Chem. Rev. 96*, 2889−2907.

(3) Kaila, V. R., Verkhovsky, M. I., and Wikström, M. (2010) Proton-coupled electron transfer in cytochrome oxidase. *Chem. Rev. 110*, 7062−7081.

(4) Hemp, J., and Gennis, R. B. (2008) Diversity of the heme-copper superfamily in *Archaea*: Insights from genomics and structural modeling. *Results Probl. Cell Differ. 45*, 1−31.

(5) Pereira, M. M., Santana, M., and Teixeira, M. (2001) A novel scenario for the evolution of haem-copper oxygen reductases. *Biochim. Biophys. Acta 1505*, 185−208.

(6) Soulimane, T., Buse, G., Bourenkov, G. P., Bartunik, H. D., Huber, R., and Than, M. E. (2000) Structure and mechanism of the aberrant ba_3-cytochrome *c* oxidase from *Thermus thermophilus*. *EMBO J. 19*, 1766−1776.

(7) Buschmann, S., Warkentin, E., Xie, H., Langer, J. D., Ermler, U., and Michel, H. (2010) The structure of cbb_3 cytochrome oxidase provides insights into proton pumping. *Science 329*, 327−330.

(8) Han, H., Hemp, J., Pace, L. A., Ouyang, H., Ganesan, K., Roh, J. H., Daldal, F., Blanke, S. R., and Gennis, R. B. (2011) Adaptation of aerobic respiration to low O_2 environments. *Proc. Natl. Acad. Sci. U.S.A. 108*, 14109−14114.

(9) Oshima, T., and Imahori, K. (1974) Description of *Thermus thermophilus* comb. nov., a nonsporulating thermophilic bacterium from a Japanese thermal spa. *Int. J. Syst. Bacteriol. 24*, 102−112.
(10) Radzi Noor, M., and Soulimane, T. (2012) Bioenergetics at extreme temperature: *Thermus thermophilus* ba_3- and caa_3-type cytochrome *c* oxidases. *Biochim. Biophys. Acta 1817*, 638−649.
(11) Zimmermann, B. H., Nitche, C. I., Fee, J. A., Rusnak, F., and Münck, E. (1988) Properties of a copper-containing cytochrome ba_3: A second terminal oxidase from the extreme thermophile *Thermus thermophilus*. *Proc. Natl. Acad. Sci. U.S.A. 85*, 5779−5783.
(12) Fee, J. A., Choc, M. G., Findling, K. L., Lorence, R., and Yoshida, T. (1980) Properties of a copper-containing cytochrome c_1aa_3 complex: A terminal oxidase of the extreme thermophile *Thermus thermophilus* HB8. *Proc. Natl. Acad. Sci. U.S.A. 77*, 147−151.
(13) Keightley, J., Zimmermann, B. H., Mather, M. W., Springer, P., Pastuszyn, A., Lawrence, D. M., and Fee, J. A. (1995) Molecular genetic and protein chemical characterization of the cytochrome ba_3 from *Thermus thermophilus* HB8. *J. Biol. Chem. 270*, 20345−20358.
(14) Soulimane, T., von Walter, M., Hof, P., Than, M. E., Huber, R., and Buse, G. (1997) Cytochrome-c_{552} from *Thermus thermophilus*: A functional and crystallographic investigation. *Biochem. Biophys. Res. Commun. 237*, 572−576.
(15) Tsukihara, T., Aoyama, H., Yamashita, E., Tomizaki, T., Yamaguchi, H., Shinzawa-Itoh, K., Nakashima, R., Yaono, R., and Yoshikawa, S. (1996) The whole structure of the 13-subunit oxidized cytochrome *c* oxidase at 2.8 Å. *Science 272*, 1136−1144.
(16) Svensson-Ek, M., Abramson, J., Larsson, G., Törnroth, S., Brzezinski, P., and Iwata, S. (2002) The X-ray crystal structures of wild-type and EQ(I-286) mutant cytochrome *c* oxidases from *Rhodobacter sphaeroides*. *J. Mol. Biol. 321*, 329−339.
(17) Iwata, S., Ostermeier, C., Ludwig, B., and Michel, H. (1995) Structure at 2.8 Å resolution of cytochrome *c* oxidase from *Paracoccus denitrificans*. *Nature 376*, 660−669.
(18) Abramson, J., Riistama, S., Larsson, G., Jasaitis, A., Svensson-Ek, M., Laakkonen, L., Puustinen, A., Iwata, S., and Wikström, M. (2000) The structure of the ubiquinol oxidase from *Escherichia coli* and its ubiquinone binding site. *Nat. Struct. Biol. 7*, 910−917.
(19) Riistama, S., Puustinen, A., Verkhovsky, M. I., Morgan, J. E., and Wikström, M. (2000) Binding of O_2 and its reduction are both retarded by replacement of valine 279 by isoleucine in cytochrome *c* oxidase from *Paracoccus denitrificans*. *Biochemistry 39*, 6365−6372.
(20) Salomonsson, L., Lee, A., Gennis, R. B., and Brzezinski, P. (2004) A single-amino-acid lid renders a gas-tight compartment within a membrane-bound transporter. *Proc. Natl. Acad. Sci. U.S.A. 101*, 11617−11621.
(21) Luna, V. M., Chen, Y., Fee, J. A., and Stout, C. D. (2008) Crystallographic studies of Xe and Kr binding within the large internal cavity of cytochrome ba_3 from *Thermus thermophilus*: Structural analysis and role of oxygen transport channels in the heme-Cu oxidases. *Biochemistry 47*, 4657−4665.
(22) Luna, W. M., Fee, J. A., Deniz, A. A., and Stout, C. D. (2012) Mobility of Xe atoms within the oxygen diffusion channel of cytochrome ba_3 oxidase. *Biochemistry 51*, 4669−4676.
(23) Hofacker, I., and Schulten, K. (1998) Oxygen and proton pathways in cytochrome *c* oxidase. *Proteins: Struct., Funct., Genet. 30*, 100−107.
(24) Einarsdottir, Ó., Funatogawa, C., Soulimane, T., and Szundi, I. (2012) Kinetic studies of the reactions of O_2 and NO with reduced *Thermus thermophilus* ba_3 and bovine aa_3 using photolabile carriers. *Biochim. Biophys. Acta 1817*, 672−679.
(25) Szundi, I., Funatogawa, C., Fee, J. A., Soulimane, T., and Einarsdóttir, Ó. (2010) CO impedes superfast O_2 binding in ba_3 cytochrome oxidase from *Thermus thermophilus*. *Proc. Natl. Acad. Sci. U.S.A. 107*, 21010−21015.
(26) Chen, Y., Hunsicker-Wang, L., Pacoma, R. L., Luna, E., and Fee, J. A. (2005) A homologous expression system for obtaining engineered cytochrome ba_3 from *Thermus thermophilus* HB8. *Protein Expression Purif. 40*, 299−318.
(27) Caffrey, M., and Cherezov, V. (2009) Crystallizing membrane proteins using lipidic mesophases. *Nat. Protoc. 4*, 706−731.
(28) Cheng, A., Hummel, B., Qiu, H., and Caffrey, M. (1998) A simple mechanical mixer for small viscous lipid-containing samples. *Chem. Phys. Lipids 95*, 11−21.
(29) Tiefenbrunn, T., Liu, W., Chen, Y., Katritch, V., Stout, C. D., Fee, J. A., and Cherezov, V. (2011) High resolution structure of the ba_3 cytochrome *c* oxidase from *Thermus thermophilus* in a lipidic environment. *PLoS One 6*, e22348.
(30) Battye, T. G., Kontogiannis, L., Johnson, O., Powell, H. R., and Leslie, A. G. (2011) iMOSFLM: A new graphical interface for diffraction-image processing with MOSFLM. *Acta Crystallogr. D67*, 271−281.
(31) McCoy, A. J., Grosse-Kunstleve, R. W., Adams, P. D., Winn, M. D., Storoni, L. C., and Read, R. J. (2007) Phaser crystallographic software. *J. Appl. Crystallogr. 40*, 658−674.
(32) Murshudov, G. N., Skubak, P., Lebedev, A. A., Pannu, N. S., Steiner, R. A., Nicholls, R. A., Winn, M. D., Long, F., and Vagin, A. A. (2011) REFMAC5 for the refinement of macromolecular crystal structures. *Acta Crystallogr. D67*, 355−367.
(33) Georgiadis, K. E., Jhon, N.-I., and Einarsdóttir, Ó. (1994) Time-resolved optical absorption studies of intramolecular electron transfer in cytochrome *c* oxidase. *Biochemistry 33*, 9245−9256.
(34) Hug, S. J., Lewis, J. W., Einterz, C. M., Thorgeirsson, T. E., and Kliger, D. S. (1990) Nanosecond photolysis of rhodopsin: Evidence for a new, blue-shifted intermediate. *Biochemistry 29*, 1475−1485.
(35) Szundi, I., Lewis, J. W., and Kliger, D. S. (1997) Deriving reaction mechanisms from kinetic spectroscopy. Application to late rhodopsin intermediates. *Biophys. J. 73*, 688−702.
(36) Szundi, I., Van Eps, N., and Einarsdóttir, Ó. (2003) pH dependence of the reduction of dioxygen to water by cytochrome *c* oxidase. 2. Branched electron transfer pathways linked by proton transfer. *Biochemistry 42*, 5074−5090.
(37) Muramoto, K., Hirata, K., Shinzawa-Itoh, K., Yoko-o, S., Yamashita, E., Aoyama, H., Tsukihara, T., and Yoshikawa, S. (2007) A histidine residue acting as a controlling site for dioxygen reduction and proton pumping by cytochrome *c* oxidase. *Proc. Natl. Acad. Sci. U.S.A. 104*, 7881−7886.
(38) Hunsicker-Wang, L. M., Pacoma, R. L., Chen, Y., Fee, J. A., and Stout, C. D. (2005) A novel cryoprotection scheme for enhancing the diffraction of crystals of recombinant cytochrome ba_3 oxidase from *Thermus thermophilus*. *Acta Crystallogr. D61*, 340−343.
(39) Liu, B., Chen, Y., Doukov, T., Soltis, S. M., Stout, C. D., and Fee, J. A. (2009) Combined microspectrophotometric and crystallographic examination of chemically reduced and X-ray radiation-reduced forms of cytochrome ba_3 oxidase from *Thermus thermophilus*: Structure of the reduced form of the enzyme. *Biochemistry 48*, 820−826.
(40) Pettersen, E. F., Goddard, T. D., Huang, C. C., Couch, G. S., Greenblatt, D. M., Meng, E. C., and Ferrin, T. E. (2004) UCSF chimera: A visualization system for exploratory research and analysis. *J. Comput. Chem. 25*, 1605−1612.
(41) Szundi, I., Rose, M. J., Sen, I., Eroy-Reveles, A. A., Mascharak, P. K., and Einarsdóttir, Ó. (2006) A new approach for studying fast biological reactions involving nitric oxide: Generation of NO using photolabile ruthenium and manganese NO donors. *Photochem. Photobiol. 82*, 1377−1384.
(42) Shinzawa-Itoh, K., Aoyama, H., Muramoto, K., Terada, H., Kurauchi, T., Tadehara, Y., Yamasaki, A., Sugimura, T., Kurono, S., Tsujimoto, K., Mizushima, T., Yamashita, E., Tsukihara, T., and Yoshikawa, S. (2007) Structures and physiological roles of 13 integral lipids of bovine heart cytochrome *c* oxidase. *EMBO J. 26*, 1713−1725.
(43) Qin, L., Liu, J., Mills, D. A., Proshlyakov, D. A., Hiser, C., and Ferguson-Miller, S. (2009) Redox-dependent conformational changes in cytochrome *c* oxidase suggest a gating mechanism for proton uptake. *Biochemistry 48*, 5121−5130.
(44) Koepke, J., Olkhova, E., Angerer, H., Muller, H., Peng, G., and Michel, H. (2009) High resolution crystal structure of *Paracoccus denitrificans* cytochrome *c* oxidase: New insights into the active site

and the proton transfer pathways. *Biochim. Biophys. Acta 1787*, 635−645.
(45) Lin, J. H., Perryman, A. L., Schames, J. R., and McCammon, J. A. (2002) Computational drug design accommodating receptor flexibility: The relaxed complex scheme. *J. Am. Chem. Soc. 124*, 5632−5633.
(46) Perryman, A. L., Forli, S., Morris, G. M., Burt, C., Cheng, Y., Palmer, M. J., Whitby, K., McCammon, J. A., Phillips, C., and Olson, A. J. (2010) A dynamic model of HIV integrase inhibition and drug resistance. *J. Mol. Biol. 397*, 600−615.
(47) Lu, R., Limon, A., Ghory, H. Z., and Engelman, A. (2005) Genetic analyses of DNA-binding mutants in the catalytic core domain of human immunodeficiency virus type 1 integrase. *J. Virol. 79*, 2493−2505.
(48) Koutsoupakis, C., Soulimane, T., and Varotsis, C. (2003) Docking site dynamics of ba_3-cytochrome *c* oxidase from *Thermus thermophilus*. *J. Biol. Chem. 278*, 36806−36809.